Characterisation of Sr^{2+} mobility in osteoporotic rat bone marrow by cryo-ToF-SIMS and cryo-OrbiSIMS

– Supplementary Information

Christine Kern[1], Reem Jamous[2], Thaqif El Khassawna[2], and Marcus Rohnke[1]

1. *Institute of Physical Chemistry, Justus Liebig University Giessen, Heinrich-Buff-Ring 17, 35392 Giessen, Germany*
2. *Experimental Trauma Surgery, Faculty of Medicine, Justus Liebig University Giessen, Aulweg 128, 35392 Giessen, Germany*

* Corresponding author. E-mail address: Marcus.Rohnke@phys.chemie.uni-giessen.de, Tel: ++49 641 99 34502, Fax: ++49 641 99 34509

EXPERIMENTAL

1. Preparation of cryo-sectioned rat bone samples and rat fat sections

The experimental group OVX rats received a diet deficient in several elements when compared to the group SHAM, which received a standard diet (Altromin-C1034 and C100, respectively; Altromin-Spezialfutter GmbH, Germany) (**Table S1**).

Table S1. Ingredients of both standard and multi – deficiencies diet.

Ingredients	Units	Content/normal	content / diet
Alanine	mg/kg	2528	8703.23
Aluminum	mg/kg	3.706	3.566
Arachidic C-20: 0	mg/kg	250	250
Arachidonic acid C 20: 4	mg/kg	2.5	2.5
Arginine	mg/kg	9828.79	11513.058
Aspartic acid	mg/kg	3583.14	15052.732
Behenic C-22: 0	mg/kg	250	250
Benzoic acid	mg/kg	100	100
Biotin	mg/kg	0.201	0.5
Calcium	mg/kg	9310.506	1367.728
Capric acid C-10: 0	mg/kg	2.5	2.5
Chlorine	mg/kg	3630000	3943.798
Choline chloride	mg/kg	1011.5	1002.875
Cobalt	mg/kg	0.147	0.148
Copper	mg/kg	5.751	5.366
Crude Ash	mg/kg	54943.225	20165.35

Crude Fat	mg/kg	50830	50651
Crude Fiber	mg/kg	40450	40544.725
Crude Protein	mg/kg	176115	180682.875
Cystine	mg/kg	3196.18	4033.917
Digest.Phosporus	mg/kg	7199.565	475.212
Disaccharide	mg/kg	110960.5	98216.06
Docosahexaenoic acid C22: 6	mg/kg	2.5	2.5
Eicosadienoic C-20: 2	mg/kg	250	250
Eicosaenoic acid C-20: 1	mg/kg	250	250
Eicosapentaenoic acid C20: 5	mg/kg	2.5	2.5
Energie/Metab.	kcal/kg	3518.055	3662.779
Erucic acid C-22: 1	mg/kg	2.5	2.5
Fluorine	mg/kg	4.17	3.584
Folic acid	mg/kg	10.0024	10.0006
Glutamic acid	mg/kg	23674.97	25377.87
Glycine	mg/kg	3136	5905.315
Histidine	mg/kg	5275.79	6190.55
Inositol	mg/kg	111	102.75
Iodine	mg/kg	0.514	0.396
Iron	mg/kg	178.579	179.188
Isoleucine	mg/kg	7222.82	8811.956
Lauric acid C 12: 0	mg/kg	2.5	2.5
Leucine	mg/kg	14762.77	16897.134
Linoleic C18: 2	mg/kg	35050	35050
Linolenic C18: 3	mg/kg	150	150
Lysine	mg/kg	17400.97	15933.41
Magnesium	mg/kg	683.506	666.622
Manganese	mg/kg	100.888	99.984
Margaric	mg/kg	2.5	2.5
Methionine	mg/kg	10688	7689.508
Moisture	mg/kg	81735.625	81323.725
Molybdenum	mg/kg	0.198	19.825
Myristinsäue C-14: 0	mg/kg	2.5	2.5
Nervonic C-24: 1	mg/kg	2.5	2.5
Nicotinic acid	mg/kg	50.17	50.043
Oleic acid C-18: 1	mg/kg	10950	10950
Palmitic acid C16: 0	mg/kg	2700	2700
Palmitoleic acid C-16: 1	mg/kg	2.5	2.5
Pantothenic acid	mg/kg	50.106	50.027
Pentadecanoic C-15: 0	mg/kg	2.5	2.5
Phenylalanine	mg/kg	7171.97	11759.017
Phosphorus	mg/kg	7522.765	533.069
Polysaccharide	mg/kg	471700	513151.75
Potassium	mg/kg	7088.682	5200.773
Proline	mg/kg	12762.98	9855.784
Selenium	mg/kg	0.334	0.283
Serine	mg/kg	5267.8	10880.31
Sodium	mg/kg	2488.262	2076.593
Stearic acid C-18: 0	mg/kg	1250	1250

Sulfur	mg/kg	2791.54	3180.027
Threonine	mg/kg	7154.17	8376.773
tricosanoic	mg/kg	2.5	2.5
Tryptophan	mg/kg	1976.96	2127.1
Tyrosine	mg/kg	9285.01	8266.867
Valine	mg/kg	3296.14	10181.275
Vitamin A	I.E./kg	15000	15000
Vitamin B1	mg/kg	20.04	20.01
Vitamin B12	mg/kg	0.03	0.03
Vitamin B2	mg/kg	20.322	20.081
Vitamin B6	mg/kg	15.034	15.009
Vitamin C	mg/kg	20	19.5
Vitamin D3	I.E./kg	500	0
Vitamin E	mg/kg	163.9	163.6
Vitamin K3 (as Menadione)	mg/kg	10	5
Zinc	mg/kg	29.299	31.433

2. Diffusion experiments

Rat bone marrow samples were cooled down in the load lock of the ToF.SIMS 5 instrument (IONTOF GmbH, Münster, Germany) with liquid nitrogen to stop further diffusion of Sr^{2+} ions. Sr^{2+} ions diffuse into bone marrow during the residence times of $SrCl_2$ solution on rat bone marrow, the time to remove the excess $SrCl_2$ solution, and the time it takes to introduce the sample into the load lock. Further Sr^{2+} diffusion takes place during the cooling period of the sample inside the load lock, although it will get slower with decreasing temperature, as described by the Arrhenius equation (equation S1).

$$D = D_0 \exp\left(-\frac{E_A}{RT}\right) \qquad \text{(equation S1)}$$

With:

D = diffusion coefficient (in m^2/s)
D_0 = maximal diffusion coefficient (at infinite temperature; in m^2/s)
E_A = activation energy for diffusion (in J/mol)
T = absolute temperature (in K)
R ≈ 8.31446 J/(mol·K) is the universal gas constant.

Therefore, to be able to include a realistic estimation of the total diffusion time, the duration of the cooling phase in the load lock (n=4) was determined. The obtained temperature profile within the load lock is shown in **Figure S1** (exemplarily shown for one measurement). Time of cooling from 21 °C to 10 °C lasts 30 s, with the entire cooling phase from 21 °C to 0 °C lasting 50 s. In order to minimize the error in the calculation of the diffusion coefficients, the cooling time until a temperature of 10°C is reached is included for the calculations of the diffusion

coefficients. From 21°C to 10°C, the diffusion gets slower, thus the value of diffusion coefficients we obtain by including the cooling phase into our calculations is lower than the actual value of strontium diffusion at room temperature. To minimize this discrepancy, the diffusion time from 10°C to 0°C is not included in the adjusted calculation, although strontium ions continue to diffuse into the bone marrow bulk during this period as well. Therefore, the total time used for the calculation of the diffusion coefficients is the addition of: residence time of $SrCl_2$ solution on rat bone marrow, time to remove the excess $SrCl_2$ solution, time of sample transfer into the load lock, and time of cooling phase within the load lock until 10 °C was reached.

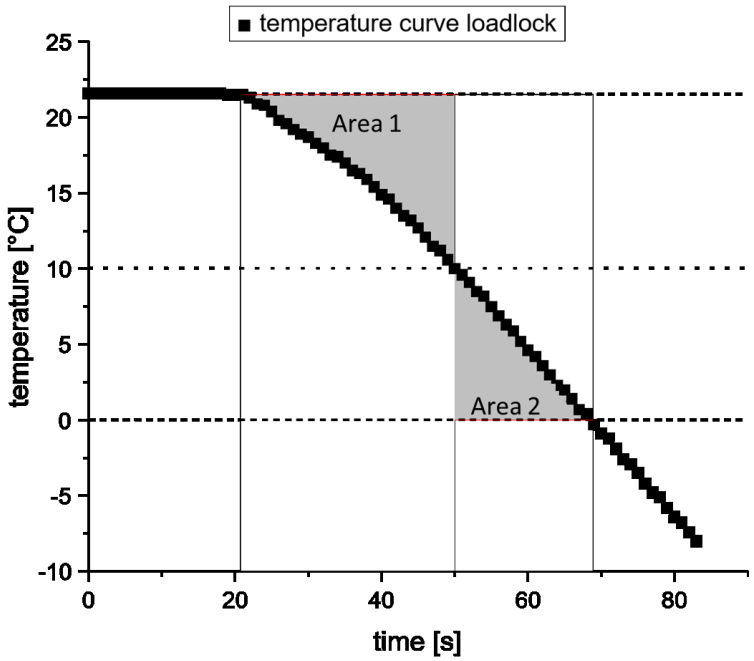

Figure S1. Temperature profile of a rat bone marrow sample inside the load lock of the ToF.SIMS 5 (IONTOF GmbH, Münster, Germany) instrument during cooling down with liquid nitrogen. Cooling time until a temperature of 10°C is reached is included for the calculations of the diffusion coefficients. The diffusion time from 10°C to 0°C is not included in the adjusted calculation.

3. Imaging analysis

a) M6 Hybrid SIMS (IONTOF GmbH, Muenster, Germany)

Table S2. Parameters for ToF-SIMS delayed extraction imaging of Sr^{2+} diffusion into rat fat sections (Figure 8, Figure S3) obtained in positive ion mode with M6 Hybrid SIMS (IONTOF GmbH, Muenster, Germany).

Figure	8 (A-D)	8 (E-H)	S3
Analysis options			
Cycle Time	130 µs	130 µs	150 µs
Field of View	500×500 µm²	150×150 µm²	300×300 µm²
Primary Ion Current	0.08 pA	0.08 pA	0.07 pA
Pixels	512×512	512×512	1024×1024
Frame per Patch	1	1	1
Primary Ion Shots/Frame/Pixel	1	1	1
Number of Scans	50	100	40

Different calibration points were selected for the high-resolution 2D imaging ($C_2H_5^+$, $C_3H_5^+$, $C_3H_7^+$, $C_5H_9^+$, $C_5H_{12}N^+$, and $C_{16}H_{31}O^+$) and depth profiling (H^+, H_2^+, CH_3^+, CH_4N^+, $C_2H_5^+$, $C_3H_7^+$, and $C_4H_8N^+$) purposes. While depth profiling was performed in spectrometry mode, high-lateral resolution imaging was performed in delayed extraction (DE) mode. Here, by turning off the extraction voltage after the primary ion pulse, in our case for 150 ns, ion extraction and secondary ion generation are decoupled and a field-free emission of secondary particles is achieved.[1] This allows secondary ions originating from the sides of the sample to drift away from the sample surface before the extraction voltage is turned on. Therefore, topographic field effects have a lesser influence on the ion extraction, fewer shadow effects occur, and sharper images are obtained.[1] At the same time, there is a significant reduction in the detectable secondary ions. This is due to the fact that only ions directly below the analyzer entrance are collected. Furthermore, fast ions of lower mass leave the extraction zone within the field-free delay time before the extraction voltage is turned on.[1] Thus, very light secondary ions (e.g., H, H_2) do not appear in the mass spectrum. For this reason, ions with higher masses have to be used for the calibration of the DE images than for the depth profiles.

RESULTS

1. Determination of Sr^{2+} diffusion coefficients in rat bone marrow

Table S3. List of positive lipid species identified in osteoporotic rat bone marrow, and rat fat sections. These listed peaks were used for Figures 3-11. For ToF imaging analysis, performed in the positive ion mode, 25 keV Bi_3^+ cluster primary ions were applied for Figure 3 (TOS.SIMS 5, IonToF GmbH, Münster, Germany), and 30 keV Bi_3^+ primary ions were applied for Figures 4, 5, 6, 9, and 10 (M6 Hybrid SIMS, IonToF GmbH, Münster, Germany). For Orbitrap imaging and spectral analysis using the OrbiTrap™ analyser, 20 keV Ar_{3000}^+ cluster primary ions were applied (Figures 7, 8, 11) (positive ion mode, obtained with M6 Hybrid SIMS). Fragments of fatty acids and lipids were based on peaks known from literature [2-6] and lipid database "The LIPID MAPS® Lipidomics Gateway" (https://www.lipidmaps.org/). FA=Fatty acid; MAG=Monoacylglycerol; DAG=Diacylglycerol; TAG=Triacylglycerol.

m/z	Peak label	Source	*m/z*	Peak label	Source
71.05	$C_4H_7O^+$	Butyric acid (FA 4:0)	309.24	$C_{19}H_{33}O_3^+$	MAG 16:2
89.06	$C_4H_9O_2^+$	Butyric acid (FA 4:0)	311.26	$C_{19}H_{35}O_3^+$	MAG 16:1
93.07	$C_7H_9^+$	Various fatty acids	312.30	$C_{20}H_{40}O_2^+$	Arachidic acid (FA 20:0)
95.09	$C_7H_{11}^+$	Various fatty acids	313.27	$C_{19}H_{37}O_3^+$	MAG 16:0 or DAG 34:1 or TAG 52:0
97.10	$C_7H_{13}^+$	Various fatty acids	335.29	$C_{22}H_{39}O_2^+$	Eicosatrienoic acid (FA 22:3)
99.08	$C_6H_{11}O^+$	Caproic acid (FA 6:0)	337.29	$C_{21}H_{37}O_3^+$	MAG 18:2
105.07	$C_8H_9^+$	Various fatty acids	339.29	$C_{21}H_{39}O_3^+$	MAG 18:1 or DAG 34:1
107.09	$C_8H_{11}^+$	Various fatty acids	341.31	$C_{21}H_{41}O_3^+$	MAG 18:0 or TAG 52:0
109.10	$C_8H_{13}^+$	Various fatty acids	365.31	$C_{23}H_{41}O_3^+$	MAG 20:0
117.09	$C_6H_{13}O^+$	Caproic acid (FA 6:0)	367.32	$C_{23}H_{43}O_3^+$	MAG 20:1
119.09	$C_9H_{11}^+$	Various fatty acids	493.43	$C_{31}H_{57}O_4^+$	DAG 28:1
127.11	$C_8H_{15}O^+$	Caprylic acid (FA 8:0)	495.44	$C_{31}H_{59}O_4^+$	DAG 28:0
143.11	$C_8H_{15}O_2^+$	Various fatty acids	517.43	$C_{33}H_{57}O_4^+$	DAG 30:3
145.12	$C_8H_{17}O_2^+$	Caprylic acid (FA 8:0)	519.44	$C_{33}H_{59}O_4^+$	DAG 30:2
155.14	$C_{10}H_{19}O^+$	Capric acid (FA 10:0)	521.46	$C_{33}H_{61}O_4^+$	DAG 30:1

173.15	$C_{10}H_{21}O_2^+$	Capric acid (FA 10:0)	523.47	$C_{33}H_{63}O_4^+$	DAG 30:0
183.17	$C_{12}H_{23}O^+$	Lauric acid (FA 12:0)	545.46	$C_{35}H_{61}O_4^+$	DAG 32:3
201.18	$C_{12}H_{25}O_2^+$	Lauric acid (FA 12:0)	547.47	$C_{35}H_{63}O_4^+$	DAG 32:2
227.20	$C_{14}H_{27}O_2^+$	Myristoleic acid (FA 14:0)	549.49	$C_{35}H_{65}O_4^+$	DAG 32:1
229.13	$C_{14}H_{29}O_2^+$	Myristic acid (FA 14:0)	551.50	$C_{35}H_{67}O_4^+$	DAG 32:0
237.22	$C_{16}H_{29}O^+$	Palmitoleic acid (FA 16:1)	571.47	$C_{37}H_{63}O_4^+$	DAG 34:4
239.24	$C_{16}H_{31}O^+$	Palmitic acid (FA 16:0)	573.49	$C_{37}H_{65}O_4^+$	DAG 34:3
243.23	$C_{15}H_{31}O_2^+$	Pentadecylic acid (FA 15:0)	575.50	$C_{37}H_{67}O_4^+$	DAG 34:2
255.23	$C_{16}H_{31}O_2^+$	Palmitoleic acid (FA 16:1)	577.52	$C_{37}H_{69}O_4^+$	DAG 34:1
257.25	$C_{16}H_{33}O_2^+$	Palmitic acid (FA 16:0)	579.53	$C_{37}H_{71}O_4^+$	DAG 34:0 or TAG 52:0
263.24	$C_{18}H_{31}O^+$	Linoleic acid (FA 18:2)	591.50	$C_{35}H_{68}O_5Na^+$	DAG 32:0
265.25	$C_{18}H_{33}O^+$	Oleic acid (FA 18:1) or DAG 34:1	597.49	$C_{39}H_{65}O_4^+$	DAG 36:5
267.27	$C_{18}H_{35}O^+$	Stearic acid (FA 18:0)	599.50	$C_{39}H_{67}O_4^+$	DAG 36:4
281.25	$C_{18}H_{33}O_2^+$	Linoleic acid (FA 18:2)	601.52	$C_{39}H_{69}O_4^+$	DAG 36:3
283.26	$C_{18}H_{35}O_2^+$	Oleic acid (FA 18:1)	603.53	$C_{39}H_{71}O_4^+$	DAG 36:2
285.28	$C_{18}H_{37}O_2^+$	Stearic acid (FA 18:0)	605.55	$C_{39}H_{73}O_4^+$	DAG 36:1
287.24	$C_{20}H_{31}O^+$	Arachidonic acid (FA 20:4)	607.56	$C_{39}H_{75}O_4^+$	DAG 36:0 or TAG 52:0
305.25	$C_{20}H_{33}O_2^+$	Arachidonic acid (FA 20:4)			

Table S4. Diffusion coefficients (± standard deviation (STD), *n*=8) for Sr^{2+} diffusion in areas of slow diffusion (SD), fast diffusion (FD), and total measurement areas (TA) of rat bone marrow. Diffusion coefficients were determined by diffusion profiles obtained with ToF-SIMS depth profiling.

Measure-ment	Slow Diffusion $D_{rat,SD}$	Fast Diffusion $D_{rat,FD}$	Total Area Diffusion $D_{rat,TA}$
	[cm²/s]	[cm²/s]	[cm²/s]
1	$3.09 \cdot 10^{-10}$	$3.15 \cdot 10^{-10}$	$3.23 \cdot 10^{-10}$
2	$4.52 \cdot 10^{-10}$	$4.60 \cdot 10^{-10}$	$4.78 \cdot 10^{-10}$
3	$4.83 \cdot 10^{-10}$	$6.46 \cdot 10^{-10}$	$6.74 \cdot 10^{-10}$
4	$1.29 \cdot 10^{-9}$	$1.90 \cdot 10^{-9}$	$1.84 \cdot 10^{-9}$
5	$5.56 \cdot 10^{-10}$	$1.03 \cdot 10^{-9}$	$9.52 \cdot 10^{-10}$
6	$1.61 \cdot 10^{-10}$	$3.57 \cdot 10^{-10}$	$3.55 \cdot 10^{-10}$
7	$8.85 \cdot 10^{-10}$	$1.11 \cdot 10^{-10}$	$1.11 \cdot 10^{-10}$
8	$1.05 \cdot 10^{-9}$	$1.42 \cdot 10^{-9}$	$1.38 \cdot 10^{-9}$
Mean value ± STD	$\mathbf{(6.48 \pm 3.88) \cdot 10^{-10}}$	$\mathbf{(9.05 \pm 5.64) \cdot 10^{-10}}$	$\mathbf{(8.89 \pm 5.37) \cdot 10^{-10}}$

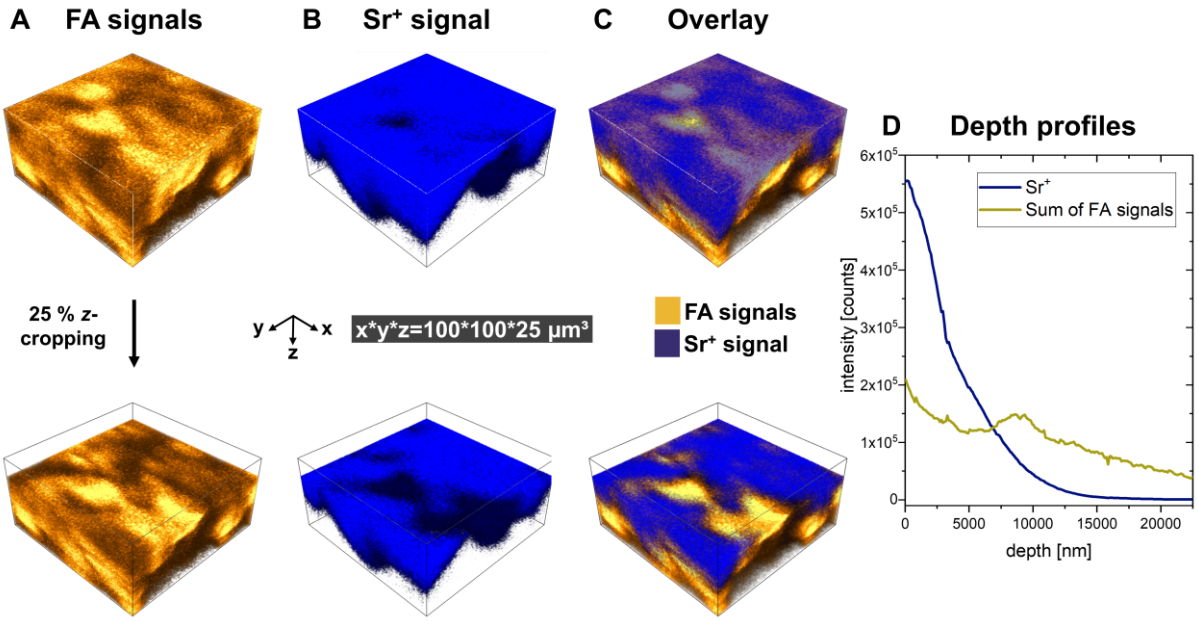

Figure S2. Reconstructed 3D mass images of **A)** FA signals, **B)** strontium signal, and **C)** overlay of FA signals in yellow and strontium in blue show Sr^{2+} diffusion into rat bone marrow at the surface and in the bulk at 25 % *z*-cropping. **D)** Diffusion profiles show the in-depth distribution of Sr^{2+} in rat bone marrow as well as distribution of fatty acids. Fatty acid signals are detectable from the beginning, thus excluding a possible formation of salt crust on the surface due to excessive strontium. For 3D imaging analysis and diffusion profiles, 25 keV Bi_3^+ cluster primary ions were applied in spectrometry mode (positive ion mode, obtained with TOF.SIMS 5).

2. ToF-SIMS imaging of strontium distribution in rat bone marrow

Table S5. Secondary ions originating from hydroxyapatite (HAP, $Ca_{10}(PO_4)_6(OH)_2$) identified in femur rat bone section are listed below. Fragments of HAP were assigned according to previous literature [7-10]. Analysis was performed in the positive ion mode with 30 keV Bi_3^+ primary cluster ions (positive ion mode, obtained with M6, IONTOF GmbH, Münster, Germany).

Hydroxyapatite (HAP) signals					
m/z	Peak label	*m/z*	Peak label	*m/z*	Peak label
39.96	Ca^+	112.92	$Ca_2O_2H^+$	174.88	$Ca_2PO_4^+$
55.96	CaO^+	118.92	$CaPO_3^+$	214.84	$Ca_3PO_4^+$
56.92	$CaOH^+$	134.92	$CaPO_4^+$	230.84	$Ca_3PO_5^+$
95.92	Ca_2O^+	151.88	$Ca_3O_2^+$	286.79	$Ca_4PO_6^+$
102.93	$CaPO_2^+$	158.88	$Ca_2PO_3^+$		
111.91	$Ca_2O_2^+$	168.88	$Ca_3O_3H^+$		

Table S6. Strontium mass signals identified in rat bone marrow. Analysis was performed in the positive ion mode with 30 keV Bi_3^+ primary cluster ions as analysis species (positive ion mode, obtained with M6, IONTOF GmbH, Münster, Germany).

Strontium signals					
m/z	Peak label	*m/z*	Peak label	*m/z*	Peak label
85.91	$^{86}Sr^+$	103.90	SrO^+	156.87	$^{87}SrCl_2^+$
86.91	$^{87}Sr^+$	104.91	$SrOH^+$	157.87	$SrCl_2^+$
87.91	Sr^+	120.88	$^{86}SrCl^+$	158.88	$SrCl_2H^+$
88.91	SrH^+	122.87	$SrCl^+$		
102.91	$^{87}SrO^+$	124.87	$Sr^{37}Cl^+$		

High-resolution ion images (**Figure S3**) of smaller areas of bone marrow from the femur section of **Figure 4** were obtained with delayed extraction mode. Combination of secondary ions originating from fatty acids (**Figure S3 C**, **G**, **K**) as well as from mono- and diacylglycerols (MAGs, DAGs) (**Figure S3 D**, **H**, **L**) show a complementary lateral distribution to strontium signals (**Figure S3 B**, **F**, **J**). In overlay images, strontium signals are mainly detectable in areas

where the intensity of FA signals is low and vice versa (**Figure S3 A**, **E**, **I**; FA signals are shown in yellow; Sr signals are shown in blue). Used mass signals for FAs, MAGs, and DAGs are listed in Table S3, strontium mass signals are listed in Table S6.

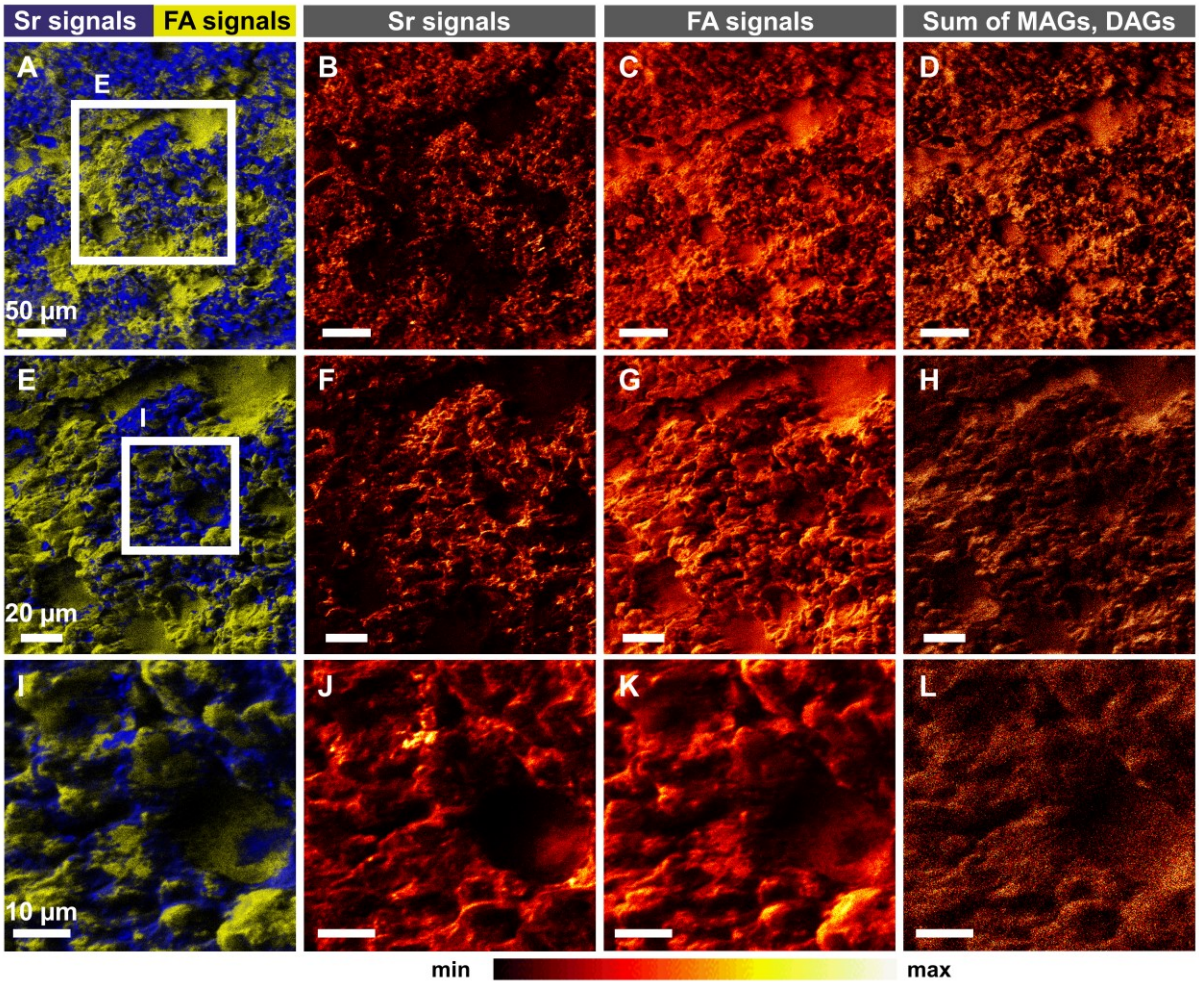

Figure S3. High-resolution ToF-SIMS images of Sr^{2+} diffusion into osteoporotic rat bone marrow. **A**, **E**, **I)** In detailed, high-resolution overlay images, secondary ions which are derived from fatty acids (yellow) show a complementary lateral distribution as the strontium signals (blue). **B)** Lateral distribution of combined strontium mass fragments (more detailed **F**, **J**) show high intensity only in certain areas of bovine bone marrow. **C)** Summed signals from secondary ions which originated from FA fragments (more detailed **G**, **K**) and **D)** from mono- and diacylglycerols (MAGs, DAGs) (more detailed **H**, **L**) show complementary distribution to strontium mass signals. Used mass signals for FAs, MAGs, and DAGs are listed in Table S3, strontium mass signals are listed in Table S6. For high-resolution imaging analysis, 30 keV Bi_3^+ cluster primary ions were applied in delayed extraction mode (positive ion mode, obtained with M6 Hybrid SIMS).

3. Sr^{2+} diffusion in rat fat sections

PCA analysis allowed statistical differentiation between areas with high intensity of strontium signals and areas with high intensity of FA/lipid signals (**Figure S4**). **Figure S4 D** shows the PCA scores image of PC1 with positive loading fragments (**Figure S4 G**) found for ion species such as $^{87}Sr^+$ (*m/z* 86.91), Sr^+ (*m/z* 87.91), SrH^+ (*m/z* 88.91), $SrOH^+$ (*m/z* 104.91), and $SrCl^+$ (*m/z* 122.86). Image scores for PC1 show the same pattern as ion image of strontium signals (**Figure S4 A**). In comparison, **Figure S4 E** shows the PCA scores image of PC2 with positive loading fragments (**Figure S4 H**) mainly found for ion species originating from fragments of MAGs (e.g., $C_{19}H_{37}O_3^+$ (*m/z* 313.27), $C_{21}H_{39}O_3^+$ (*m/z* 339.29)) and DAGs (e.g., $C_{33}H_{63}O_4^+$ (*m/z* 523.47), $C_{35}H_{67}O_4^+$ (*m/z* 551.50), $C_{37}H_{67}O_4^+$ (*m/z* 575.50), $C_{39}H_{69}O_4^+$ (*m/z* 601.52)). Positive loadings of PC2 scores image (red) shows the same pattern as the mass image for FA signals (**Figure S4 B**). Negative loadings for PC2 (blue in the corresponding scores image) include mainly masses of strontium fragments. Therefore, these mass fragments are anti-correlated to the PC2 image score. Overlay of PC1 (blue) and PC2 (positive loadings are shown in yellow) scores images (**Figure S4 F**) captures the variation between areas of fast Sr^{2+} diffusion and high fatty acid intensity and is comparable with the overlay of strontium (blue) and fatty acid (yellow) signals (**Figure S4 C**).

Peaks identified with OrbiSIMS analysis are listed in **Table S7**. For comparison of mass accuracy between the OrbiTrap™ and the ToF analyser (ToF-SIMS measurement from **Figure 8**), the deviations of the assigned masses from the theoretical masses are listed. Especially for the inorganic strontium peaks, a better mass accuracy could be achieved with the Orbitrap analyser. Deviation obtained with the Orbitrap analyser was for all selected peaks < 5 ppm (for most selected peaks < 2 ppm). In comparison, deviation obtained with the ToF analyser was > 45 ppm for inorganic strontium species and > 20 ppm for lipid peaks on average. Mass resolution of signals obtained with OrbiTrap™ analyser was also higher than mass resolution obtained with the ToF analyser. For inorganic strontium species, mass resolutions >100,000 could be obtained with OrbiTrap™ analyser (>2,000 up to >4,000 with ToF analyser). For MAGs and DAGs, mass resolutions from >40,000 up to >50,000 were achieved (ToF-analyser: >5,000).

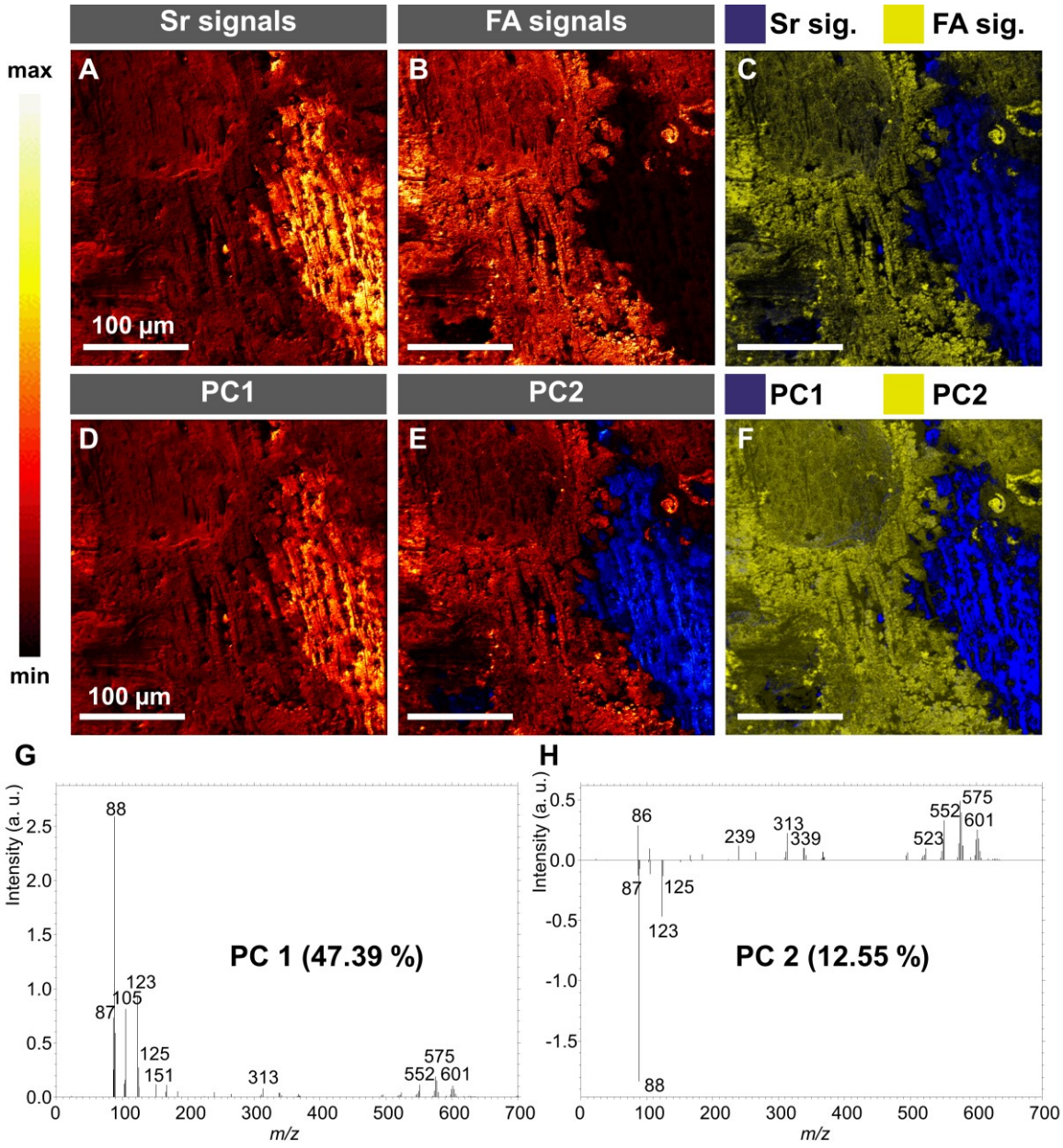

Figure S4. Comparison of ToF-SIMS mass images of secondary ions originating from **A)** strontium fragments, **B)** fatty acid/lipid species of rat fat section, and **C)** overlay of strontium signals (blue) and FA signals (yellow) with Principal Component Analysis (PCA) scores images (**D-F**) and loadings plots (**G**, **H**). **D)** PCA scores image of PC1 with G) corresponding loadings plot. **E)** PCA scores image of PC2 with H) corresponding loadings plot. **F)** Overlay image of PC1 (blue) and PC2 (yellow). 30 keV Bi_3^+ cluster primary ions were applied (positive ion mode, delayed extraction, obtained with M6 Hybrid SIMS).

Table S7. List of positive lipid and strontium species identified in rat fat sections with M6 Hybrid SIMS instrument using OrbiTrap™ or ToF analyser. Deviations show the values in ppm by which the assigned masses deviate from the theoretical masses, respectively. Orbitrap analysis (from Figure 9): 20 keV Ar_{3000}^+ primary ion clusters as analysis species. ToF analysis (from Figure 8): 30 keV Bi_3^+ cluster as primary ions, delayed extraction mode. Fragments of MAGs and DAGs were assigned according to literature[66]. MAG=Monoacylglycerol; DAG=Diacylglycerol.

m/z	Peak label	Deviation OrbiTrap™ Analyser [ppm]	Deviation ToF-Analyser [ppm]	Mass resolution OrbiTrap™ Analyser	Mass resolution ToF-Analyser	Description
85.9089	$^{86}Sr^+$	2.1	-73.8	>100,000	>2,000	Strontium (Sr) isotope
86.9085	$^{87}Sr^+$	2.3	-66.4	>100,000	>2,000	Sr isotope
87.9052	Sr^+	2.0	-45.5	>100,000	>2,000	Sr isotope
104.9078	$SrOH^+$	-0.1	-121.2	>100,000	>4,000	Sr fragment
122.8738	$SrCl^+$	-1.0	-117.4	>80,000	>4,000	Sr fragment
124.8709	$Sr^{37}Cl^+$	-0.8	-114.5	>80,000	>4,000	Sr fragment
313.2733	$C_{19}H_{37}O_3^+$	-1.2	-13.3	>50,000	>4,000	MAG 16:0
337.2741	$C_{21}H_{37}O_3^+$	1.2	-30.0	>50,000	>5,000	MAG 18:2
339.2893	$C_{21}H_{39}O_3^+$	-0.2	-34.3	>50,000	>5,000	MAG 18:1
523.4715	$C_{33}H_{63}O_4^+$	-1.1	-9.7	>40,000	>5,000	DAG 30:0
547.4708	$C_{35}H_{63}O_4^+$	-2.3	-24.2	>50,000	>5,000	DAG 32:2
549.4869	$C_{35}H_{65}O_4^+$	-1.5	-17.3	>50,000	>5,000	DAG 32:1
551.5027	$C_{35}H_{67}O_4^+$	-1.3	-14.8	>50,000	>5,000	DAG 32:0
573.4868	$C_{37}H_{65}O_4^+$	-1.6	-23.4	>40,000	>5,000	DAG 34:3
575.5026	$C_{37}H_{67}O_4^+$	-1.3	-18.9	>40,000	>5,000	DAG 34:2
577.5180	$C_{37}H_{69}O_4^+$	-1.8	-19.1	>40,000	>5,000	DAG 34:1
579.5319	$C_{37}H_{71}O_4^+$	-4.8	-19.5	>40,000	>5,000	DAG 34:0
597.4865	$C_{39}H_{65}O_4^+$	-2.1	-38.0	>40,000	>5,000	DAG 36:5
599.5026	$C_{39}H_{67}O_4^+$	-1.3	-35.3	>40,000	>5,000	DAG 36:4
601.5181	$C_{39}H_{69}O_4^+$	-1.5	-32.1	>40,000	>5,000	DAG 36:3
603.5333	$C_{39}H_{71}O_4^+$	-2.3	-27.4	>40,000	>5,000	DAG 36:2
605.5473	$C_{39}H_{73}O_4^+$	-4.9	-23.0	>40,000	>5,000	DAG 36:1

DISCUSSION

Table S8. Diffusion coefficients of water in bone marrow, obtained with diffusion-weighted magnetic resonance imaging (DW-MRI) compared to values for Sr^{2+} ion diffusion in rat bone marrow determined in this study as well as in bovine bone marrow determined in a previous study with ToF-SIMS, respectively.

Species	Sample state	Diffusion species	Technique	*D* [cm²/s]	Reference
osteoporotic rat	in vivo	water	DW-MRI	$4 \cdot 10^{-6}$	Liu et al., 2013, [11]
human knee	in vivo	water	DW-MRI	$1.5 \cdot 10^{-6}$	Ward et al., 2000, [12]
human vertebrae	in vivo	water	DW-MRI	$(2 – 6) \cdot 10^{-6}$	Dietrich et al., 2017, [13] (data from 24 studies)
rat	-	Sr^{2+} ions	estimated	$1 \cdot 10^{-8}$	Rohnke et al., 2017, [14]
bovine	ex vivo	Sr^{2+} ions	cryo-ToF-SIMS	*Fast diffusion* $(2.09 \pm 2.39) \cdot 10^{-9}$ *Slow diffusion* $(1.52 \pm 1.80) \cdot 10^{-10}$ *Total area* $(1.94 \pm 2.40) \cdot 10^{-9}$	Kern et al., 2022, [15]
osteoporotic rat femur	ex vivo	Sr^{2+} ions	cryo-ToF-SIMS	*Fast diffusion* $(9.05 \pm 5.64) \cdot 10^{-10}$ *Slow diffusion* $(6.48 \pm 3.88) \cdot 10^{-10}$ *Total area* $(8.89 \pm 5.37) \cdot 10^{-10}$	current study

1. Henss, A., et al., *High resolution imaging and 3D analysis of Ag nanoparticles in cells with ToF-SIMS and delayed extraction.* Biointerphases, 2018. **13**(3): p. 03B410.
2. Gulin, A.A., et al., *Applicability of TOF-SIMS for the assessment of lipid composition of cell membrane structures.* Biochemistry (Moscow), Supplement Series A: Membrane and Cell Biology, 2017. **11**(2): p. 144-150.
3. Malmberg, P., et al., *Imaging of lipids in human adipose tissue by cluster ion TOF-SIMS.* Microsc Res Tech, 2007. **70**(9): p. 828-35.
4. Li, H.W., et al., *Investigation of Lipid Metabolism in Dynamic Progression of Coronary Artery Atherosclerosis of Humans by Time-of-Flight Secondary Ion Mass Spectrometry.* Anal Chem, 2021. **93**(8): p. 3839-3847.
5. Passarelli, M.K. and N. Winograd, *Lipid imaging with time-of-flight secondary ion mass spectrometry (ToF-SIMS).* Biochim Biophys Acta, 2011. **1811**(11): p. 976-90.
6. Nygren, H., et al., *Localization of cholesterol, phosphocholine and galactosylceramide in rat cerebellar cortex with imaging TOF-SIMS equipped with a bismuth cluster ion source.* Biochim Biophys Acta, 2005. **1737**(2-3): p. 102-10.
7. Kern, C., et al., *New insights into ToF-SIMS imaging in osteoporotic bone research.* Biointerphases, 2020. **15**(3): p. 031005.
8. Henss, A., et al., *Applicability of ToF-SIMS for monitoring compositional changes in bone in a long-term animal model.* J R Soc Interface, 2013. **10**(86): p. 20130332.
9. Henss, A., et al., *Quantification of calcium content in bone by using ToF-SIMS--a first approach.* Biointerphases, 2013. **8**(1): p. 31.
10. Aranyosiova, M., et al., *Strontium distribution in bones and tissues of strontium ranelate-administrated rats.* Surface and Interface Analysis, 2011. **43**(1-2): p. 306-309.
11. Liu, Y., et al., *Quantitative assessment of microcirculation and diffusion in the bone marrow of osteoporotic rats using VCT, DCE-MRI, DW-MRI, and histology.* Acta Radiol, 2013. **54**(2): p. 205-13.
12. Ward, R., et al., *Analysis of Diffusion Changes in Posttraumatic Bone Marrow Using Navigator-Corrected Diffusion Gradients.* American Journal of Roentgenology, 2000. **174**(3): p. 731-734.
13. Dietrich, O., et al., *Diffusion imaging of the vertebral bone marrow.* NMR Biomed, 2017. **30**(3).
14. Rohnke, M., et al., *Strontium release from Sr2+–loaded bone cements and dissipation in healthy and osteoporotic rat bone.* J Control Release, 2017. **262**.
15. Kern, C., A. Pauli, and M. Rohnke, *Determination of Sr2+ mobility in viscous bovine bone marrow by cryo-time-of-flight secondary ion mass spectrometry.* Rapid Communications in Mass Spectrometry, 2022. **n/a**(n/a): p. e9300.